Fatigue of rubber-modified epoxies: effect of particle size and volume fraction

H. R. AZIMI, R. A. PEARSON*, R. W. HERTZBERG
Department of Materials Science and Engineering, Polymer Interfaces Center, Materials Research Center, 5 Whitaker Laboratory, Lehigh University, Bethlehem, PA 18015, USA

A change in crack-tip plastic zone/rubber particle interactions induces a transition in the fatigue crack propagation (FCP) behaviour of rubber-modified epoxy polymers. The transition occurs at a specific K level, K_T, which corresponds to the condition where the size of the plastic zone is of the order of the size of the rubber particles. At $\Delta K > \Delta K_T$, rubber-modified epoxies exhibit improved FCP resistance compared to the unmodified epoxy. This is because the size of the plastic zone becomes large compared to the size of the rubber particles and, consequently, rubber cavitation/shear banding and plastic void growth mechanisms become active. At $\Delta K < \Delta K_T$, both neat and rubber-modified epoxies exhibit similar FCP resistance because the plastic zone size is smaller than the size of the rubber particles and hence, the rubber cavitation/shear banding and plastic void growth mechanisms are not operating. As a result of these interactions, the use of smaller 0.2 μm rubber particles in place of 1.5 μm rubber particles results in about one order of magnitude improvement in FCP resistance of the rubber-modified system, particularly near the threshold regime. Such mechanistic understanding of FCP behaviour was employed to model the FCP behaviour of rubber-modified epoxies. It is shown that the near threshold FCP behaviour is affected by the rubber particle size and blend morphology but not by the volume fraction of the modifiers. On the other hand, the slope of the Paris–Erdogan power law depends on the volume fraction of the modifiers and not on the particle size or blend morphology.

1. Introduction

McGarry and co-workers [1, 2] were among the first to show that the fracture resistance of epoxy polymers could be enhanced by the incorporation of a dispersed rubbery phase. Since their initial investigations, several studies [3–11] have provided a detailed description of the micro-deformation mechanisms responsible for the increase in fracture toughness of rubber-modified epoxy polymers. The most commonly cited mechanisms include: (i) localized shear yielding which refers to shear banding in the epoxy matrix that occurs between adjacent rubber particles; (ii) hole or plastic void growth in the epoxy matrix, initiated by cavitation or debonding of the rubber particles; and (iii) rubber particle bridging behind the crack tip. Parenthetically speaking, it is well accepted that in moderately cross-linked epoxy polymers, matrix shear yielding contributes the most to toughness improvements [3, 5–10].

Rubber-particle size is a material parameter that influences both the fracture toughness [4, 5, 10, 12–14] and the operative toughening mechanisms in rubber-modified epoxy polymers [10]. The most recent findings for rubber-modified epoxy polymers suggest the use of an optimal particle size in the range from 0.1–5 μm [10]. This observation cannot be fully explained by the interparticle distance model of Wu and Margolina [13, 14]. In a recent study, Pearson and Yee [10], while not refuting the interparticle distance model, used an argument of particle–plastic zone interaction to explain the effect of particle size on toughness of rubber-modified epoxies. These investigators claimed that particles smaller than the size of the plastic zone of the neat epoxy are more efficient toughening agents because they can interact with the crack-tip plastic zone and, thereby, cavitate and promote shear yielding mechanisms. It was proved that particles larger than the size of the plastic zone of the neat epoxy do not enhance the shear yielding in the matrix at the crack tip but simply bridge the two crack surfaces. Note that crack surface bridging by larger rubber particles is far less effective in enhancing the toughness of rubber-modified epoxies than the case where smaller particles cavitate and promote matrix shear yielding.

Increasing interest in epoxy-based composites for structural components exposed to cyclic loads necessitates the understanding of damage accumulation and

---

*Author to whom all correspondence should be addressed.

associated fracture mechanisms. However, in contrast to the case of monotonic loading, such understanding of crack-tip shielding mechanisms in toughened epoxy polymers under cyclic loading conditions, is almost non-existent. Yet, it has been shown that the failure micromechanisms and fracture surfaces generated by stable fatigue crack propagation (FCP), even in a tension /tension mode, may reveal significantly different features from those under monotonic loading conditions [15]. Furthermore, the earlier investigations of the fatigue of toughened epoxy polymers [16–20] focused mainly on the macroscopic FCP behaviour in the relatively high crack-growth rate regime $(\mathrm{d}a/\mathrm{d}N > 10^{-4}\,\mathrm{mm\,cycle^{-1}})$ and did not elucidate crack-tip shielding mechanisms. An understanding of the crack-tip shielding mechanisms in the low crack-growth rate regime is of paramount importance because the near-threshold behaviour may be life-controlling in many applications, especially in the case of brittle polymers [21]. Moreover, near-threshold data for polymer matrices are rare [22]. Therefore, it is of great interest to study the effect of rubber-modification on the FCP behaviour and on the crack-tip shielding mechanisms at both low and high crack-growth rate regimes. Obviously, such information is required for the development of a satisfactory model for the FCP behaviour of rubber-modified epoxy polymers.

In a previous communication [23], the importance of rubber particle–plastic zone interactions on the toughening mechanisms in a rubber-modified DGEBA-based epoxy subjected to cyclic loading was reported. It was shown that such interactions result in a transition (ΔK_T) in the FCP behaviour of rubber-modified epoxy, below which, both neat and rubber-modified epoxies exhibit similar FCP resistance. Furthermore, it was shown that this transition phenomenon occurs when the size of the crack-tip plastic zone is of the order of the size of the rubber particles (see Fig. 1).
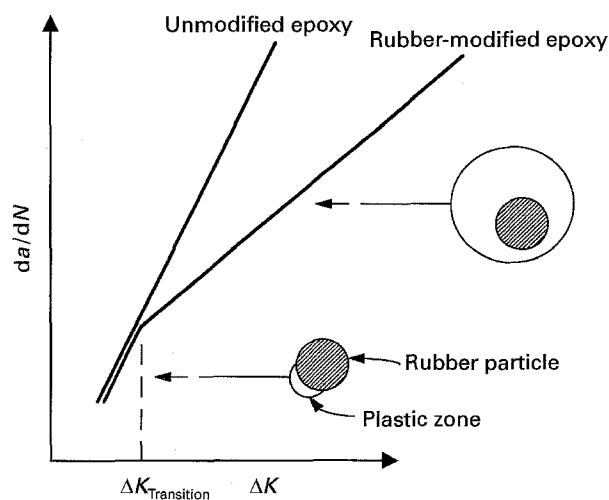

Figure 1 A schematic drawing showing the transition phenomenon observed in the FCP behaviour of rubber-modified epoxies. Note that below the transition, ΔK_T, both neat and modified epoxies exhibit similar FCP resistance.

3778

Because the size of the rubber particles and the surface-to-surface interparticle distance in that particular rubber-modified epoxy were almost the same, it is appropriate to question whether the transition phenomenon is related to interparticle distance rather than to particle size considerations. The object of this study was to gain a better understanding of such transition behaviour by changing the volume fraction and the size of the rubber particles. Furthermore, the implication of our findings in modelling the FCP behaviour of these materials will be discussed.

2. Experimental procedure
2.1. Preparation of the model epoxy system
The epoxy matrices used for this system are two types of diglycidyl ether of bisphenol A epoxy resins with an equivalent weight of $187\,\mathrm{g\,mol^{-1}}$, DER® 331 resin from Dow Chemical Company, or $500–560\,\mathrm{g\,mol^{-1}}$, DER® 661 resin from Dow Chemical Company, designated DGEBA-187 or DGEBA-550, respectively. Three kinds of rubber modifiers were employed: a liquid carboxyl-terminated butadiene–acrylonitrile (CTBN) copolymer (Hycar® 1300 X8 from B. F. Goodrich); structured core–shell latex particles comprised of a methacrylated butadiene–styrene copolymer (MBS) with a few per cent carboxyl groups (COOH) included in the poly(methyl methacrylate) (PMMA) shell (Paraloid® EXL-2691 additive from Rohm and Haas Company); and MBS particles (Paraloid® EXL-2611 additive from Rohm and Haas Company). In this study, these three types of rubber were designated CTBN, MBS-COOH, and MBS, respectively. Note that a few per cent of carboxyl (COOH) groups included in the methyl methacrylated shell should improve the dispersion of the particles in the epoxy resin. The CTBN rubber phase separated from the epoxy matrix during cure, resulting in particles ranging from $1–1.5\,\mu\mathrm{m}$ in diameter for the DGEBA-1 system (increasing in size with increasing volume fraction). The size of the phase-separated CTBN rubber particles in the DGEBA-2 epoxy system is about $3\,\mu\mathrm{m}$. The commercially available MBS particles have a pre-determined size of $0.2\,\mu\mathrm{m}$. The formulations of the materials are shown in Table I.

For the DGEBA-187 epoxy system, plaques of rubber-modified epoxy polymers were prepared using the following procedure. First, 500 g DGEBA-187 epoxy resin were degassed at $80\,^\circ\mathrm{C}$ with agitation. Next, liquid CTBN rubber or solid MBS particles were added and the epoxy mixture again degassed with agitation. Piperidine (29 ml) was added to this epoxy mixture at ambient pressure. This curing agent/epoxy resin mixture was degassed once again with slow agitation and poured into a pre-heated Teflon-coated aluminium mould at $120\,^\circ\mathrm{C}$. The mould was then placed in a circulating air oven to cure for 16 h at $120\,^\circ\mathrm{C}$. The procedure for preparing DGEBA-550 epoxy system is the same as above, except for the amount of curing agent (11 ml) and the curing schedule (16 h at $160\,^\circ\mathrm{C}$).

TABLE I Formulations of the rubber-modified epoxies studied

Designation	Resin (g)	Piperidine (ml)	Rubber (g)	Particle size (μm)
DGEBA-187[a]	500	29	0.0	0.0
DGEBA-550	500	11	0.0	0.0
DGEBA-187/CTBN(1)[b]	500	29	5	1.0
DGEBA-187/CTBN(5)	500	29	25	1.3
DGEBA-187/CTBN(10)	500	29	50	1.5
DGEBA-187/MBS-COOH(5)	500	29	25	0.2
DGEBA-187/MBS-COOH(10)	500	29	50	0.2
DGEBA-187/MBS(10)	500	29	50	0.2
DGEBA-550/CTBN(10)	500	11	50	3.0

[a] For a description of the types of the epoxy resin and the rubber, see the text.
[b] Numbers in parenthesis denote the volume fraction of the modifier.

2.2. Mechanical testing

2.2.1. Tensile testing

Tensile tests were performed on type-I specimens (ASTM D638 Standard) at a crosshead speed of $10 \, mm \, min^{-1}$, using a screw-driven Instron testing machine. The reported tensile strengths represent averages of three tests; specimens either fractured or yielded. A type-D 1 in gauge extensometer was used to determine the nominal strain which allowed for the calculation of the tensile modulus of the materials.

2.2.2. Fracture toughness testing

Fracture toughness measurements were performed on precracked, single-edge notched (SEN) specimens (see Fig. 2) in three-point bend (3PB) geometry and in accordance with the ASTM D5045 standard. Precracking was performed by tapping a cold razor blade (immersed in liquid nitrogen) into the machined notch provided in the specimens. Tests were conducted on a screw-driven Instron 1011 materials testing machine with a crosshead speed of $2 \, mm \, min^{-1}$. Equation 1 (ASTM D5045-91) was used to calculate K_{IC} from sample/pre-crack dimensions and sample deformation behaviour.

$$K_{IC} = \frac{3PSa^{0.5}}{2tw^2} f(a/w) \tag{1}$$

where P is the critical load for crack propagation (N); S the length of span (mm); a the precrack length (mm); t, the thickness (mm); w the width (mm); and $f(a/w)$ a non-dimensional shape factor

$$f(a/w) = 1.9 - 3.07 \, (a/w) + 14.53 \, (a/w)^2$$
$$- 25.11 \, (a/w)^3 - 25.80 \, (a/w)^4 \tag{2}$$

The fracture toughness values (reported in Table II) represent averages of five to eight tests, and were obtained under plane strain condition.

2.2.3. Fatigue crack propagation

Fatigue crack propagation (FCP) studies were performed using notched compact tension (CT) specimens (see Fig. 2), in general accordance with the ASTM Standard E647-93 recommended practice.
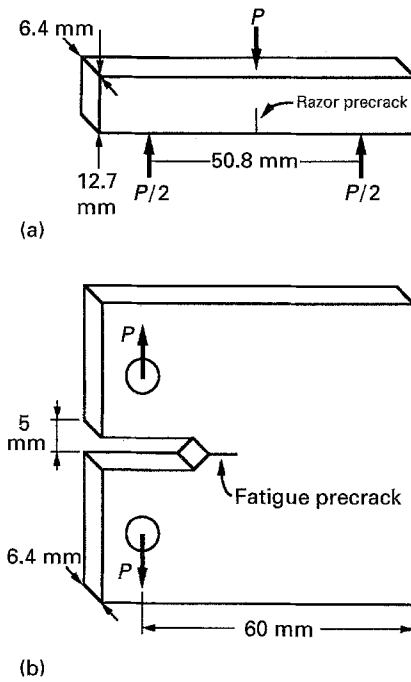

Figure 2 The dimensions of (a) SEN and (b) CT specimens used in this study.

Specimens were cyclically loaded at ambient conditions. A computer-controlled Instron servo-hydraulic materials testing machine was used to apply a sinusoidal frequency of 10 Hz with a load ratio (R = minimum load/maximum load or $R = K_{min}/K_{max}$) of 0.1.

Crack-growth data were obtained by interfacing the Instron machine to a desktop computer and using software and hardware developed by Fracture Technology Associates, Inc. On-line crack-length monitoring was performed via measurement of the instantaneous compliance of the specimen with a crack opening displacement (COD) gauge that was attached to knife edges located in the mouth of the notch of the CT specimens. Crack growth rates, da/dN, were determined from compliance-inferred crack-length measurements and associated number of cycles, N, using a modified secant formulation

$$\left(\frac{da}{dN}\right)_n = \frac{a_{n+1} - a_{n-1}}{N_{n+1} - N_{n-1}} \tag{3}$$

TABLE II Tensile Young's modulus, E, yield strength, α_y, plane-strain fracture toughness, K_{IC}, and rubber particle size for the rubber-modified epoxies

Compositions Pip +	E (GPa)	α_y (MPa)	K_{IC} (MPa m$^{0.5}$)	Particle size (μm)
DGEBA-187	3.00	74.0	0.86 ± 0.02	0.0
DGEBA-550	2.94	71.2	0.9 ± 0.03	0.0
DGEBA-187/CTBN(1)	2.92	72.6	1.05 ± 0.03	~ 1.0
DGEBA-187/CTBN(5)	2.80	67.0	1.69 ± 0.04	~ 1.3
DGEBA-187/CTBN(10)	2.60	61.0	2.02 ± 0.02	~ 1.5
DGEBA-187/MBS-COOH(5)	2.83	70.7	2.10 ± 0.03	~ 0.2
DGEBA-187/MBS-COOH(10)	2.61	65.0	2.11 ± 0.03	~ 0.2
DGEBA-187/MBS(10)	2.60	54.0	2.80 ± 0.06	~ 0.2
DGEBA-550/CTBN(10)	2.53	56.6	3.20 ± 0.04	~ 3.0
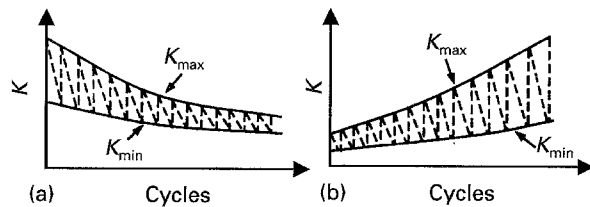
Figure 3 A schematic drawing representing (a) R-constant decreasing ΔK and (b) R-constant increasing ΔK test methodologies used in the present work.

where a is the crack length, n an iteration number, and N the number of cycles.

In order to avoid any load interaction, precracking of CT specimens was performed under constant load conditions such that the final K_{max} of the precracking procedure was less than the initial K_{max} of the decreasing ΔK portion of the test.

Crack-growth data were first generated under decreasing ΔK conditions (Fig. 3) using an automated load-shedding scheme given by Equation 4

$$\Delta K = \Delta K_0 \exp[C^*(a - a_0)] \qquad (4)$$

where ΔK is the instantaneous value of stress intensity factor range $(K_{max} - K_{min})$, a the instantaneous value of crack length, ΔK_0 the initial value of stress intensity range, a_0 the initial value of crack length, and C^* the normalized stress intensity gradient $[(dK/da)/K]$, and by setting C^* to $- 0.08$ mm^{-1} crack extension. After reaching a crack growth rate of about 10^{-6} mm cycle^{-1}, tests were continued under increasing ΔK conditions (Fig. 3) by setting C^* to $+ 0.08$ mm^{-1}. Crack-growth data were plotted against ΔK, the range in the applied stress intensity factor. Stress intensities were calculated by the software and from standard solutions for the compact geometry (ASTM E399-93).

2.3. Fractography
2.3.1. Optical microscopy
Optical microscopy (OM) was employed to examine the nature of sub-surface fatigue damage in the crack wake and at the crack tip of the compact tension specimens. For this purpose, thin sections in the range 150–200 and 30–50 μm from the crack regions (plane strain sections, see Fig. 4) were prepared using
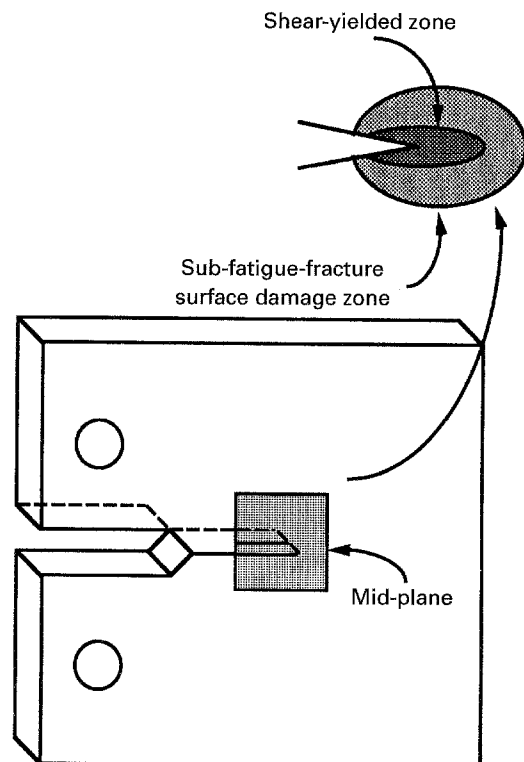

Figure 4 A schematic drawing showing the position from where the OM samples were obtained.

petrographic polishing techniques [15]. These thin sections were viewed on a Zeiss optical microscope under transmitted light (TOM); both bright-field or crossed-polarized viewing conditions were used.

2.3.2. Scanning electron microscopy
A JEOL 6300F low-voltage scanning electron microscope (SEM) was used to examine the fatigue fracture surfaces of the materials tested. All fracture surfaces were coated prior to fractography unless otherwise mentioned. A thin layer of gold–palladium, sputtered on the fracture surface, reduced the amount of the charge build-up in the sample. Scanning electron micrographs were obtained under conventional secondary electron imaging conditions and with an accelerating voltage of 5 kV.

2.3.3. Transmission electron microscopy

These experiments were kindly performed by Dr H.-J. Sue and co-workers at Dow Chemical Company in Freeport Texas. Transmission electron microscopy (TEM) samples were prepared to investigate further the nature of fatigue-induced damage in the process zone surrounding the crack. For this purpose, the sub-surface damage zone about 100 μm beneath the fracture surface was carefully trimmed to an appropriate size, i.e. an area of ≈ 5 mm $\times$ 5 mm, and then embedded in DER® 331 epoxy resin/diethylene triamine (12:1 ratio by weight) following exposure at 38 °C for 16 h. The cured block was then further trimmed to a size of ≈ 0.3 mm $\times$ 0.3 mm with the region of interest in the damage zone roughly at the centre of the trimmed surface. A glass knife was used to face off the trimmed block prior to OsO$_4$ staining. Regarding the latter, the faced-off block was placed in a vial containing 1 g 99.9% pure OsO$_4$ crystals and stained for 16 h. Ultra-thin sections, ranging from 60–80 nm, were obtained using a Reichert-Jung Ultracut E microtome with a diamond knife. The thin sections were placed on 200-mesh formvar-coated copper grids and examined using the JEOL 2000FX ATEM operated at an accelerating voltage of 100 kV.

3. Results and discussion
3.1. Fatigue crack propagation: transition phenomenon

Tensile and fracture toughness data for the materials studied are given in Table II. Crack-growth rate, da/dN, data versus crack driving force, ΔK, for the control material (DGEBA-550) and for the epoxy polymer containing 10 vol% CTBN rubber are plotted in Fig. 5. As can be seen from this figure, the FCP resistance of rubber-modified epoxy is relatively insensitive to the modifier content at low ΔK levels. However, above a ΔK level of about 0.55 MPa m$^{0.5}$ (hereafter, referred to as the transition point, ΔK_T), the rubber-modified epoxy polymer shows higher FCP resistance when compared to the unmodified epoxy. Using McClintock and Irwin's formula [24] for the size of the plastic zone corresponding to plane strain conditions (Equation 5), it is found that the unique value of ΔK_T corresponds to the point where the plastic-zone size is of the order of the size of the rubber particles.

$$r_y = \frac{1}{6\pi}\left(\frac{K}{\sigma_y}\right)^2 \qquad (5)$$

where r_y represents the radius of the plastic zone and K and α_y represent the maximum stress intensity at the transition point and the tensile yield strength of the neat epoxy, respectively. Such calculations reveal that the size of the plastic zone is about 3.5 μm at the empirically determined transition point, ΔK_T. Because the average size of the rubber particles is about 3 μm, (for 10 vol% rubber), it is reasonable to believe that these particles are not interacting with the crack tip when ΔK is smaller than the ΔK_T. That is, we surmise that when the plastic zone size, r_y, is greater than the

rubber particle diameter, cavitation/shear banding mechanisms are activated, thereby resulting in improved FCP resistance for the rubber-modified material. This hypothesis is confirmed in Section 3.4 through analysis of the fatigue fracture surfaces of this material for ΔK levels below and above ΔK_T.

To investigate further the occurrence of the transition phenomenon, the FCP experiments were repeated, but this time for a lower molecular weight resin (DGEBA-187 as opposed to DGEBA-550) modified by 10% CTBN rubber. The FCP results for this material are shown in Fig. 6. As can be seen from this figure, similar to the result obtained for DGEBA-550 system, the FCP resistance of rubber-modified epoxy is relatively insensitive to the modifier content at low ΔK levels. However, above a ΔK level of about 0.4 MPa m$^{0.5}$, the rubber-modified epoxy polymer shows higher FCP resistance when compared to the unmodified epoxy. If the argument of plastic zone and rubber particle interactions is used, it is found that the unique value of ΔK_T corresponds to the point where the plastic-zone size (using Equation 5) is of the order
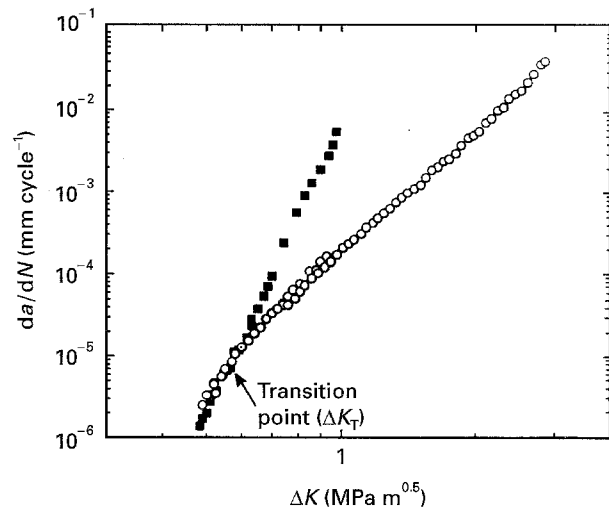

Figure 5 The effect of rubber modification on the FCP behaviour of a DGEBA-550 epoxy polymer. Note that the FCP resistance of the modified epoxy is improved when $\Delta K > \Delta K_T$. (■) unmodified, (○) modified CTBN (10%).
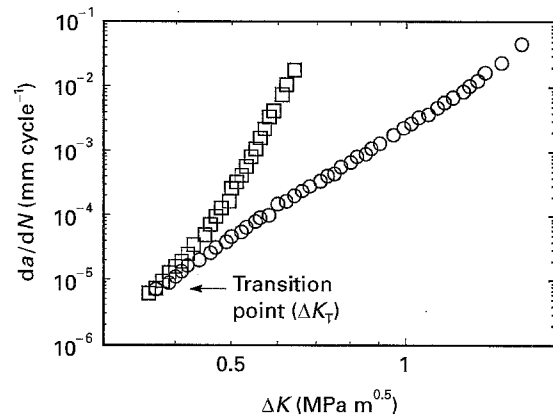

Figure 6 The effect of rubber modification on the FCP behaviour of a DGEBA-187 epoxy polymer. Note that similar to the case for DGEBA-550 (Fig. 5), the FCP resistance of the modified epoxy is improved when $\Delta K > \Delta K_T$. (□) unmodified, (○) modified CTBN (10%). $r_y = (1/6\pi)\,(K/\alpha_y)^2$ [24] ; at transition, $r_y = 1.8$ μm.

of the size of the rubber particle. Such calculations reveal that the size of the plastic zone is about 2 μm at the empirically determined transition point ($\Delta K_T = 0.4$ MPa m$^{0.5}$) . Because the average size of the rubber particles in this 10 vol% rubber system is about 1.5 μm (see Table II), it is reasonable to believe that these particles, again, are not interacting with the crack tip when $\Delta K < \Delta K_T$. Similar transition behaviour has been reported for the case of metals and particulate metal–matrix composites [25–27]. These transitions have been attributed to interactions between the cyclic plastic zone and the grain size, precipitate spacing, or particle spacing in metal alloys. Therefore, a reasonable question arises and relates to whether the transition observed in this study is related to the interparticle spacing or to the particle size. One notes that for 10% modifier, particle spacing is equal to particle size. This issue is addressed in the following section.

3.2. The effect of particle size and interparticle spacing on FCP resistance

In order to investigate the effect of interparticle spacing on the transition point in rubber-modified epoxy, CTBN rubber-modified epoxy polymers were prepared while using three different volume fractions of 1%, 5%, and 10% CTBN rubber. Formulations, as well as tensile and fracture toughness data, for these materials can be found in Tables I and II, respectively. The FCP results for these compositions are shown in Fig. 7. By changing the volume fraction of the CTBN rubber from 1% to 10%, the size of the precipitated rubber particles in the matrix remains almost constant (1–1.5 μm), whereas the "idealized" surface-to-surface interparticle distance, *ID*, changes from 4.1 μm to 0.7 μm (see Table II) using the following equation [28]

$$ID = \left[\frac{4}{3}\pi r_p^3 \left(\frac{V_m}{V_p} + 1\right)\right]^{1/3} - 2r_p \qquad (6)$$

where r_p, V_m, and V_p are the radius of the particles, volume fraction of the matrix, and volume fraction of the particles, respectively. This equation gives *ID* values that are reasonably close to the mean particle spacing found on the polished surface of the materials. As can be seen from Fig. 7, the transition point does not change with rubber volume fraction. In fact, if the transition point were a function of interparticle distance, the transition for epoxy modified by 1% rubber would have occurred at a K level of about 0.66 MPa m$^{0.5}$ which corresponds to a ΔK of 0.6 MPa m$^{0.5}$. However, as can be seen from Fig. 7, at a ΔK of 0.6 MPa m$^{0.5}$, the FCP resistance of epoxy modified by 1% CTBN is already improved by about one order of magnitude when compared to that of neat epoxy. Therefore, we strongly believe that the transition point is controlled by the rubber particle size and not by the interparticle distance.

Interestingly, whereas the particle spacing and the volume fraction of the rubber has no effect on the FCP resistance at ΔK levels below ΔK_T, they strongly affect da/dN when $\Delta K > \Delta K_T$.

According to the transition hypothesis, smaller particles should result in higher FCP resistance, particularly at low ΔK levels (i.e. in the near threshold regime). To test this hypothesis, 0.2 μm core–shell latex particles, comprised of a methacrylated butadiene–styrene (MBS) with a few per cent carboxyl (COOH) groups included in the PMMA shell, were used in place of CTBN rubber particles (1.5 μm). A solvent-exchange process was conducted to ensure the uniform dispersion of the MBS-COOH particles in the epoxy matrix. A uniform distribution of the particles in the matrix is needed if the argument of the interactions between the plastic zone and the rubber particles is to be used. The FCP results for MBS-COOH-modified epoxy are shown in Fig. 8, along with results for CTBN-modified epoxy. As can be seen from this figure, the fatigue crack-growth resistance of MBS-COOH-modified epoxy in the threshold regime is improved by about seven times when compared to that of CTBN-modified epoxy. Because the
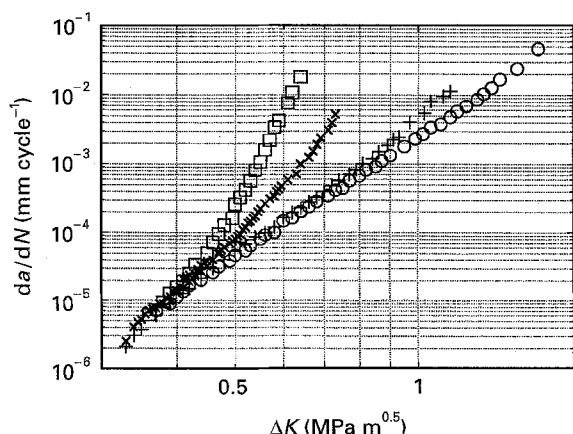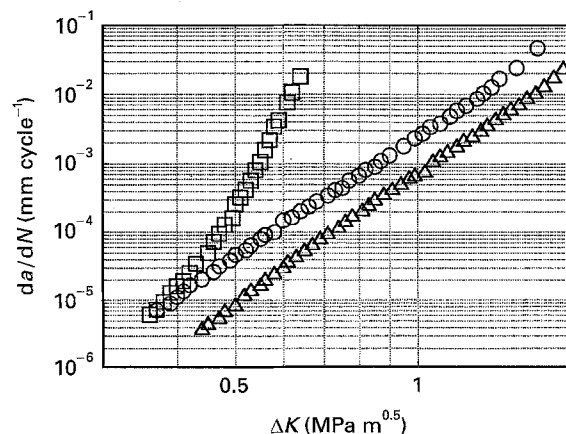

Figure 7 The effect of rubber volume fraction on the FCP behaviour of a DGEBA-187 epoxy polymer. Note that the rubber volume fraction affects the slope of the da/dN versus ΔK plot, but has no effect on the transition point. (□) unmodified, and modified CTBN: (×) 1%, (+) 5%, (○) 10%.

Figure 8 The effect of rubber-particle size on the FCP behaviour of a DGEBA-187 epoxy polymer. Note that the FCP resistance of MBS-COOH-modified epoxy has improved about seven times when compared to that of CTBN-modified epoxy. (□) unmodified, (○) modified CTBN (10%), (△) modified MBS-COOH (10%).
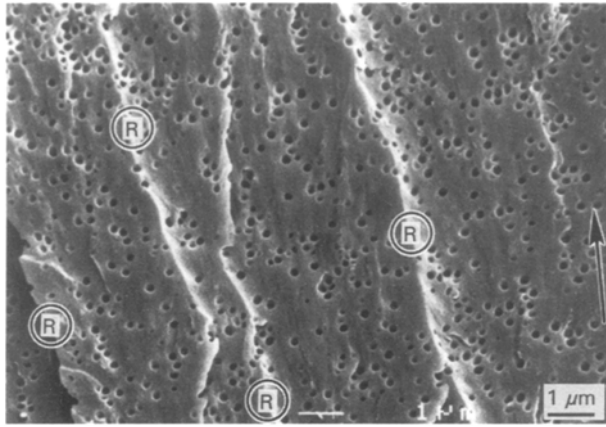
Figure 9 Scanning electron micrograph from the fatigue-fracture surfaces of a DGEBA-187/MBS-COOH(10) modified epoxy. Note that the distribution of the rubber particles is uniform.

near-threshold behaviour may be life-controlling in many applications in brittle polymers, such improvement in FCP resistance at the near-threshold regime is important. It is interesting to note that the fracture toughness of CTBN and MBS-COOH modified materials are nearly identical (Table II). Also, it is noteworthy that the fatigue fracture surface of the MBS-COOH-modified epoxy reveals that the rubber particles are uniformly distributed in the matrix (see Fig. 9).

3.3. Implications in modelling FCP behaviour

Previous work by our group [19] suggests that the FCP resistance in rubber-modified epoxy polymers increases with increasing fracture toughness. For this, Hwang *et al.* [19] showed that in the relatively high crack-growth rate regime, there is a linear correlation between ΔK^* (the driving force required to generate an arbitrary growth rate of $\mathrm{d}a/\mathrm{d}N = 7.5 \times 10^{-4}$) and K_{IC} for different rubber-modified epoxies. The question may arise that if such a simple correlation always exists, what then is the importance of the particle–plastic zone interaction in modelling the FCP behaviour of these materials? To investigate further the relation between K_{IC} and ΔK^*, a plot of ΔK^* versus K_{IC} was generated from the data in Fig. 10 and from the data of rubber-modified DGEBA-550 (Fig. 5) for two growth rates of 7.5×10^{-4} and 1×10^{-5} (see Fig. 11). The results in Fig. 11 show that at high growth rates, ΔK^* is a strong function of K_{IC}, but not at low growth rates. Indeed, linear regression of the data sets revealed correlation coefficients, R, of 0.97 and 0.7 for high and low growth rates, respectively. Furthermore, a careful examination of low growth-rate data in Fig. 11 reveals that these data can be divided into two data sets: one for 1.5 μm rubber particles and the other for 0.2 μm rubber particles. Note that the slope of the ΔK^* versus K_{IC} for these two sets are almost zero. The zero slope indicates that the FCP behaviour at the near threshold regime is not a function of K_{IC}; instead, the near-threshold FCP resistance is very sensitive to the rubber-particle size
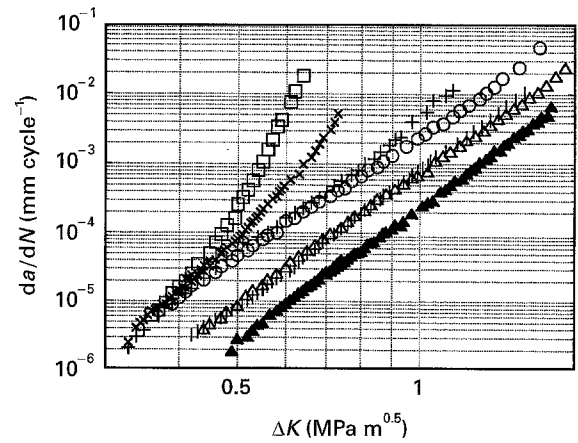

Figure 10 The FCP data for the DGEBA-187 epoxy system. Note that the smaller MBS particles are more efficient in improving FCP resistance than the larger CTBN particles. (□) unmodified; modified CTBN, (×) 1%, (+) 5%, (○) 10%; modified MBS-COOH, (|) 5%, (△) 10%; (▲) modified MBS (10%).
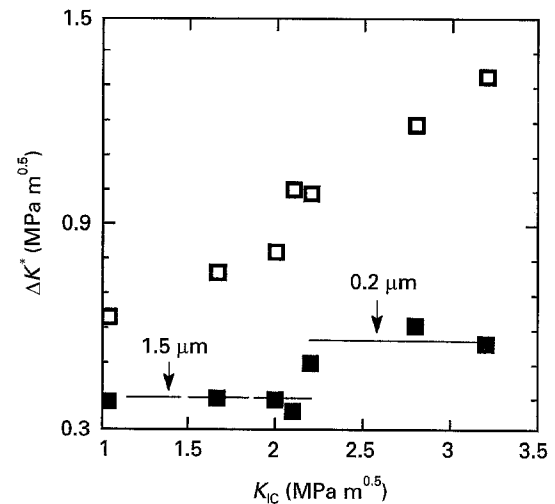

Figure 11 A plot of ΔK^* (ΔK at an arbitrary growth rate) versus K_{IC}. Note that at high growth rates, ΔK^* is a strong function of K_{IC} but at low growth rates, it is not. Indeed, linear-fits to the data sets revealed correlation coefficients, R of 0.97 and 0.7 for high growth rates and low growth rates, respectively. (□) $\Delta K^* = \Delta K$ at $\mathrm{d}a/\mathrm{d}N = 7.5 \times 10^{-4}$; (■) $\Delta K^* = \Delta K$ at $\mathrm{d}a/\mathrm{d}N = 1 \times 10^{-5}$.

(Figs 10 and 11). However, as can be seen from Fig. 10, rubber particle size has no effect on the slope of the power-law regime (*m* in Equation 7). This is consistent with previous findings [23, 25–27, 29] that in the near-threshold region, changes to the microstructure of the materials generally produce strong effects, whereas in the Paris power-law regime this is generally not the case

$$\mathrm{d}a/\mathrm{d}N = A\Delta K^m \tag{7}$$

(the Paris–Erdogan power law) where A, m are materials constants for given testing conditions and environment.

The recent results by Karger-Kocsis and Friedrich [20] suggest that the slope of the power-law regime (*m* in Equation 7) in DGEBA-based type epoxies modified by CTBN rubber and/or silicone rubber dispersions is a function of the modifier content. To investigate this, the slopes of the Paris regime for different

compositions were obtained from Fig. 10, and were plotted versus the volume fraction of the modifiers (see Fig. 12). Some additional data points from other references [19, 20] were included. As can be seen from this figure, m in rubber-modified epoxies is a strong function of the volume fraction of the rubbery phase. Therefore, we are in complete agreement with Karger-Kocsis and Friedrich [20].

To examine further the effect of microstructural changes on the FCP behaviour, the FCP data pairs were obtained for an epoxy modified by 10% MBS (EXL-2611) particles. The use of these MBS particles results in an interconnected morphology (see Fig. 13 and compare with Fig. 9) which, in turn, results in a lower yield strength, a higher fracture toughness (see Table II), and a higher FCP resistance (Fig. 10). Interestingly, the effect of blend morphology on FCP behaviour is very similar to the effect of rubber particle size; that is, the morphology of the blend does not affect the slope, m, but it strongly affects the intercept, A, in the Paris equation. In other words, it shifts the whole FCP data pairs to higher ΔK levels. For more detailed discussion on the effect of blend morphology
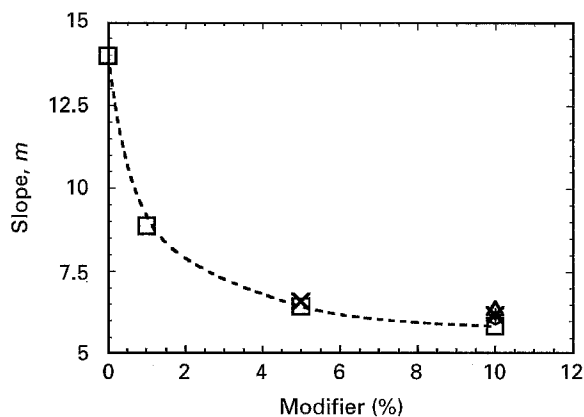

Figure 12 A plot of the slope m of the power-law regime versus the volume fraction of the modifiers. Note that the slope is independent of the rubber-particle type and size (--□--) CTBN, (-*-) MBS-COOH, (△) MBS, (○) [18], (+) [19].
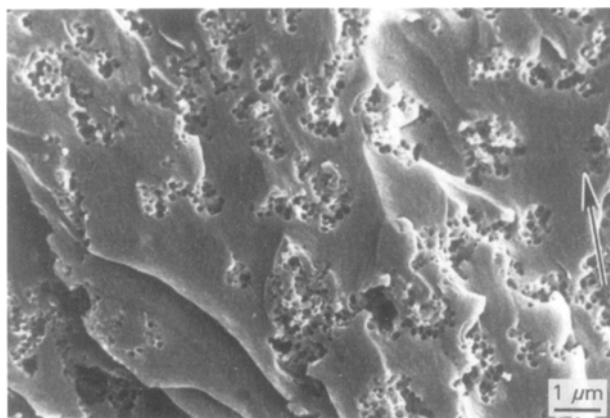

Figure 13 Scanning electron micrograph from the fatigue-fracture surfaces of DGEBA-187/Pip/MBS(10). Note the non-uniform distribution of the rubber particles in this material and compare it with Fig. 8.

on the fracture toughness of rubber-modified epoxies, the reader is referred to Bagheri [30] and Qian et al. [31].

In summary, we may conclude that rubber-particle size and blend morphology affect the FCP behaviour by affecting the pre-exponential value, A. On the other hand, the volume fraction of the modifier only affects the slope of the power-law regime. Furthermore, the near-threshold behaviour is strongly affected by rubber particle size and morphology, but not by the modifier content.

3.4. Fracture mechanisms in FCP

According to our rationale for the transition phenomenon, it is expected that the operating crack-tip shielding mechanisms would act differently at ΔK levels below and above ΔK_T. Therefore, the fatigue fracture surfaces of DGEBA-550/CTBN(10) material were examined at ΔK levels of 0.5 and 2.5 $MPa\,m^{0.5}$ and are shown in Fig. 14a and b, respectively. Fig. 14a reveals the lack of matrix plasticity for $\Delta K < \Delta K_T$ which can be attributed to the crack-tip plastic-zone size being less than the size of the rubber particles. However, this figure reveals impressions and bumps close to the centre of the rubber particles which are indicative of rubber bridging. However, by comparing the FCP results from Fig. 4 with the model suggested by Ritchie [32], one may surmise that rubber bridging, although present, is not an effective shielding mechanism (see Fig. 15). This can be attributed to the poor bridging efficiency of the rubber particles as modelled by Ahmad et al. [33]. By contrast, Fig. 14b, corresponding to $\Delta K > \Delta K_T$, reveals rubber cavitation and plastic dilation of the matrix around the cavitated rubber particles. Schematic drawings representing the toughening mechanisms at low and high ΔK levels are shown in Fig. 14c and d, respectively. The role of rubber particles in bridging the crack surfaces at $\Delta K < \Delta K_T$, and in cavitating and initiating shear yielding at $\Delta K > \Delta K_T$ is consistent with the findings in static fracture toughness testing of rubber-modified epoxy polymers [10]. As mentioned earlier, Pearson and Yee showed that rubber particles larger than the crack-tip plastic zone act as bridging agents, whereas rubber particles smaller than the crack-tip plastic zone cavitate and promote shear yielding in the matrix.

Other features shown in Fig. 14b are matrix ligaments between the cavities that are drawn in plastically and which give rise to high ridges around the cavitated rubber particles. These features, although never reported for the static fracture toughness testing of rubber-modified epoxies, seem similar to the features of the dilatational bands that were recently described by Lazzeri and Bucknall [34].

The crack-tip plastic zone–particle interaction argument suggests that when the size of the rubber particles is always smaller than the size of the plastic zone, only one fracture mechanism (cavitation/shear yielding) should be found. The size of the core–shell latex MBS-COOH rubber particles (0.2 μm) is almost one order of magnitude smaller than the size of the
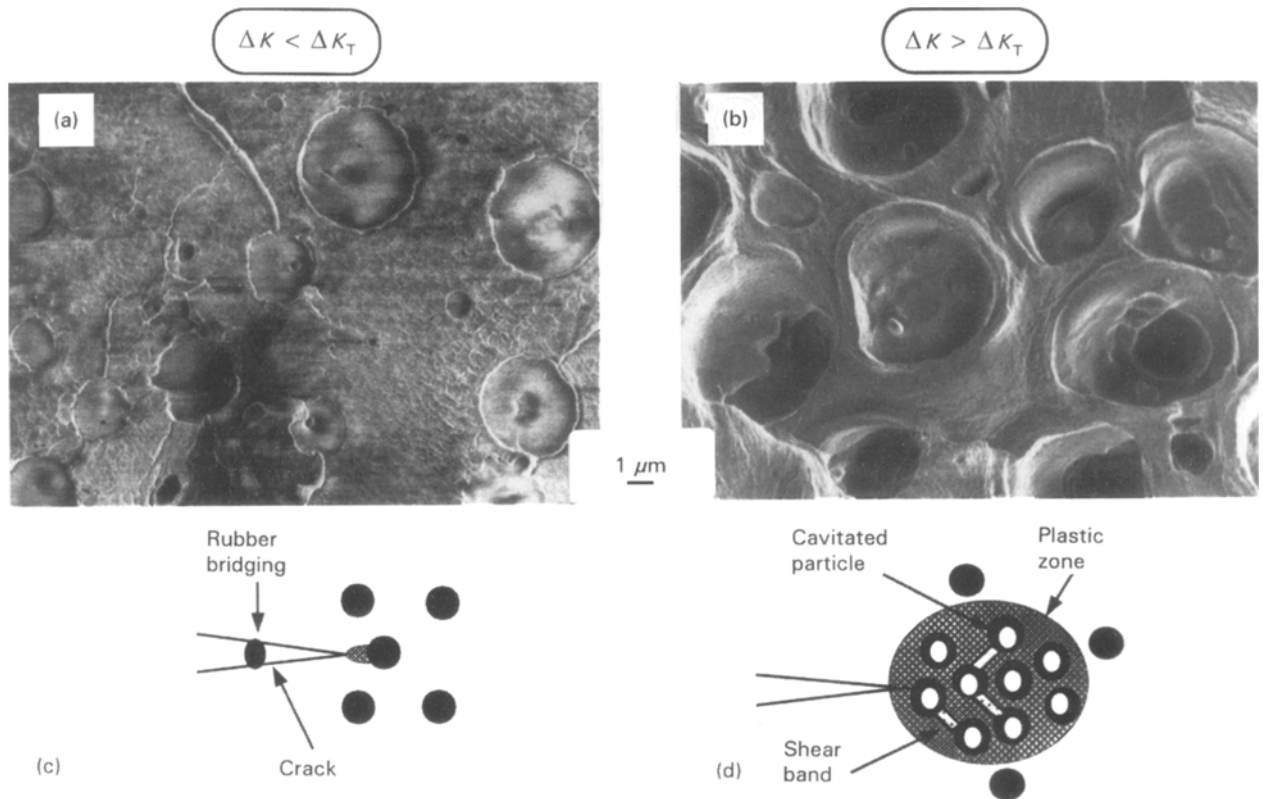
Figure 14 Scanning electron micrographs showing the fatigue-fracture surfaces of DGEBA-550/Pip/CTBN(8) at ΔK = (a) 0.5 MPa m$^{0.5}$ and (b) 2.5 MPa m$^{0.5}$. Note severe rubber cavitation and matrix dilation at high ΔK as opposed to low ΔK. Schematic drawings in (c) and (d) describe the crack-tip plastic zone–particle interactions as related to (a) and (b), respectively.
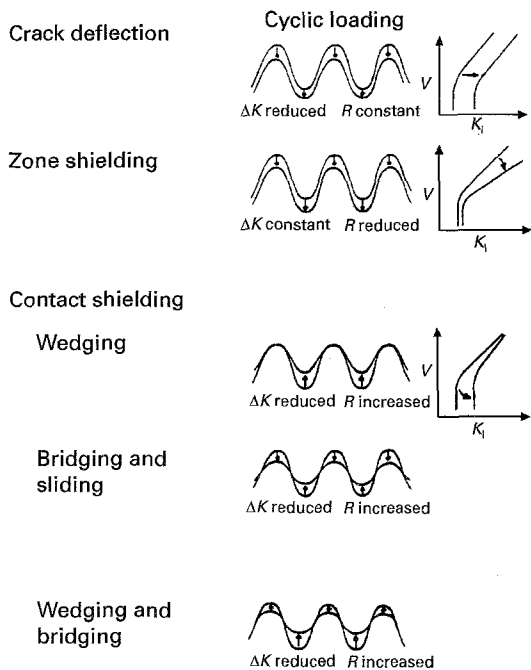

Figure 15 Schematic drawings showing the effect of specific crack-tip shielding mechanisms on crack driving force under cyclic loading [32].
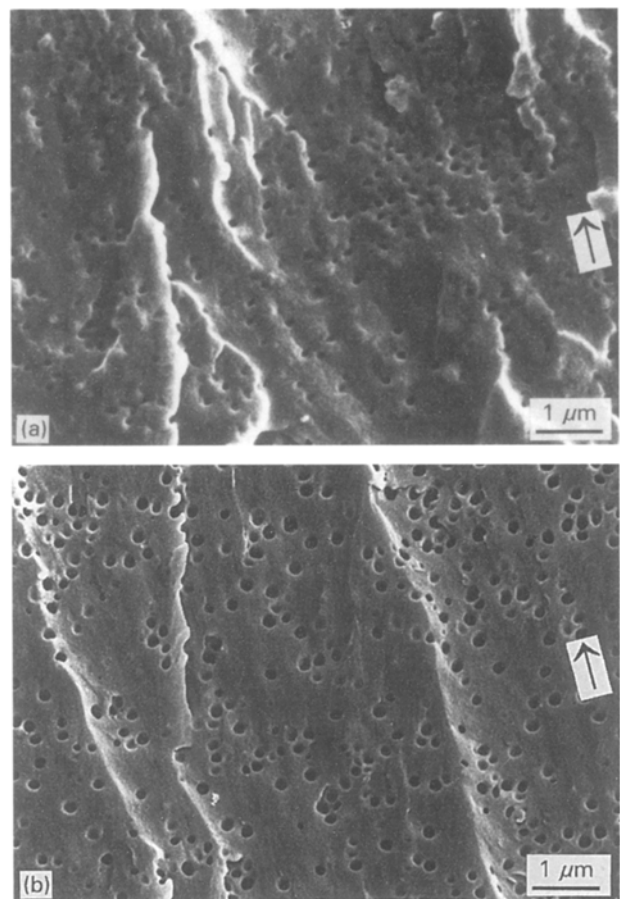

Figure 16 Scanning electron micrographs from the fatigue-fracture surfaces of DGEBA-187/Pip/MBS-COOH(10) material at ΔK = (a) 0.45 MPa m$^{0.5}$ and (b) 1.5 MPa m$^{0.5}$. Note rubber cavitation in (a) and compare it with Fig. 14a.

plastic zone (2 μm), corresponding to the lowest ΔK value (0.45 MPa m$^{0.5}$) obtained in FCP experiments for this material. As a result, the epoxy modified with 10% MBS-COOH rubber exhibits the same fatigue fracture surface appearance at ΔK levels of 0.45 and 1.5 MPa m$^{0.5}$ (Fig. 16a and b). Indeed, as can be seen

from Fig. 16a, even at low ΔK levels, these small particles have cavitated. As expected the cavitated rubber particles grew more at high ΔK level as compared with those at low ΔK level. The formation of shear ribs and steps along the crack-growth direction encouraged by cracking in different planes, can also be seen.

To elucidate further the active shielding mechanisms, the sub-surface fatigue damage of the toughest rubber-modified epoxy (DGEBA-550/CTBN(10)) was examined for $\Delta K > \Delta K_T$ conditions using optical microscopy. The results for transmitted light, both bright and crossed-polarized light viewing conditions are shown in Fig. 17a–c. From these micrographs, one sees shear banding between cavitated rubber particles (Fig. 17a and c) and the presence of a birefringent zone (Fig. 17b), indicative of matrix yielding. There are also lenticular features between rubber particles near the elastic/plastic interface that are reminiscent of crazes. A higher magnification transmission electron micrograph (Fig. 18) reveals that indeed, craze-like features are present in this material. Note that the position of the transmission electron micrograph with respect to the crack is indicated by the letter T in Fig. 17a. Although the formation of crazes in epoxy polymers is very unlikely due to their highly cross-linked structure [35], craze-like damage has been reported in association with static fracture toughness testing of rubber-modified epoxy polymers [36]. The contribution of these craze-like features on fracture toughness remains to be determined.

A mechanistic understanding of the FCP behaviour of rubber-modified thermoset polymers can, thereby, be obtained based on the crack-tip shielding mechanisms observed in Figs 14–18. The basis for crack-tip shielding under cyclic loading may take different forms. Under small-scale non-linear deformation, the fatigue-crack driving force is characterized by the range of the stress intensity factor, i.e. ΔK ($= K_{max} - K_{min}$). However, in the presence of toughening mechanisms, the driving force at the crack tip is lowered and may be written as [32]

$$\Delta K_1 = \Delta K_a - K_s \qquad (8)$$

where ΔK_1 is the local stress intensity range at the crack tip, ΔK_a is the applied stress intensity range, and K_s is the absolute changes in maximum and minimum stress intensity factors due to shielding.

Considering the model given by Ritchie [32] and the experimental results [16–20] including our results, the effect of crack-tip shielding mechanisms on the FCP behaviour of rubber-modified epoxy polymers (see Fig. 19) may be explained as follows. The addition of the compliant rubbery phase to an epoxy matrix facilitates the formation of a plastic zone through rubber cavitation/void growth and shear banding. The formation of the plastic zone shields the crack tip from the applied crack driving force by a combination of zone and contact shielding mechanisms. In other words, the formation of a plastic enclave at the crack tip produces a fixed reduction in local K_{min} and K_{max} by blunting the crack tip, which enhances the FCP resistance of the material (see Fig. 15a).
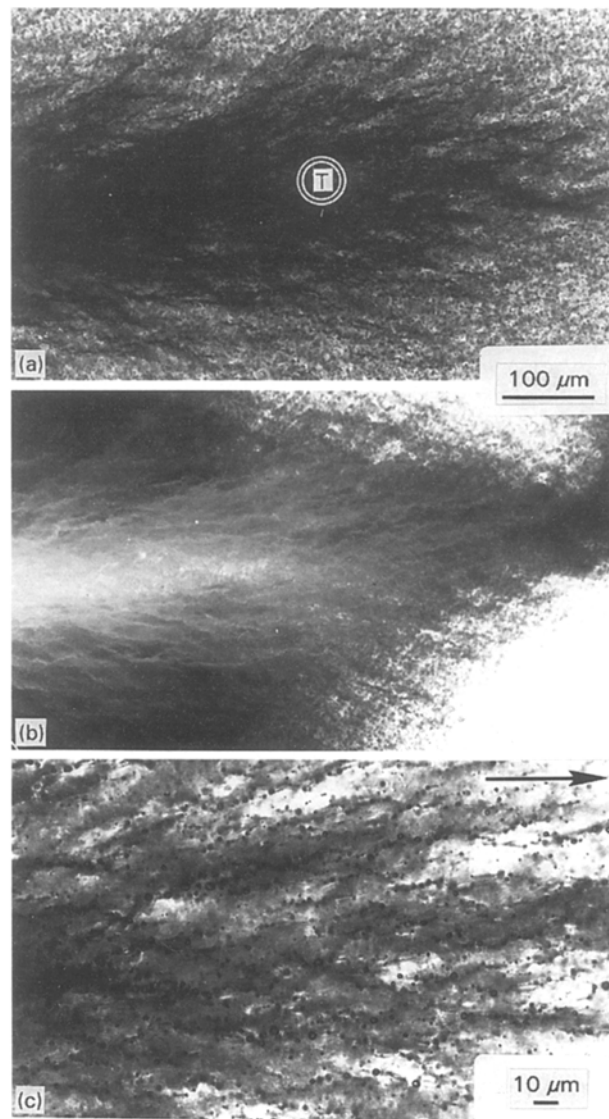

Figure 17 Optical micrographs from the sub-fatigue-fracture surfaces illustrating shear yielding in DGEBA-550/Pip/CTBN(10) material; transmitted light and bright field (a, c) and crossed polars (b). Micrographs correspond to $\Delta K = 2.5$ MPa m$^{0.5}$.

Moreover, as the crack propagates, craze-induced dilatation and dilatation induced by cavitation/void growth, enhance the FCP resistance by inducing crack closure (see Fig. 15b). Because the degree of shielding is related to the process zone size [3,10,11,29,32, 37,38], and because the size of the zone may be scaled with $(K_{max})^2$ [20], rubber toughening of epoxy is favoured at high stress intensity levels and is less potent in improving FCP resistance at low threshold regime where the plastic zone size is small.

3.5. Cavitation and plastic zone measurements

The size of the fatigue damage zone (cavitation and plastic zones) plays an important role in the transition phenomenon. In order to obtain a proper description of the fatigue damage zone in DGEBA-550/CTBN(10) rubber-modified epoxy, a fatigue crack was generated in a CT specimen of R(10) material for ΔK levels of 1, 1.5, 2 and 2.5 MPa m$^{0.5}$ which correspond to K_{max} values of 1.11, 1.67, 2.22, and 2.78 MPa m$^{0.5}$,
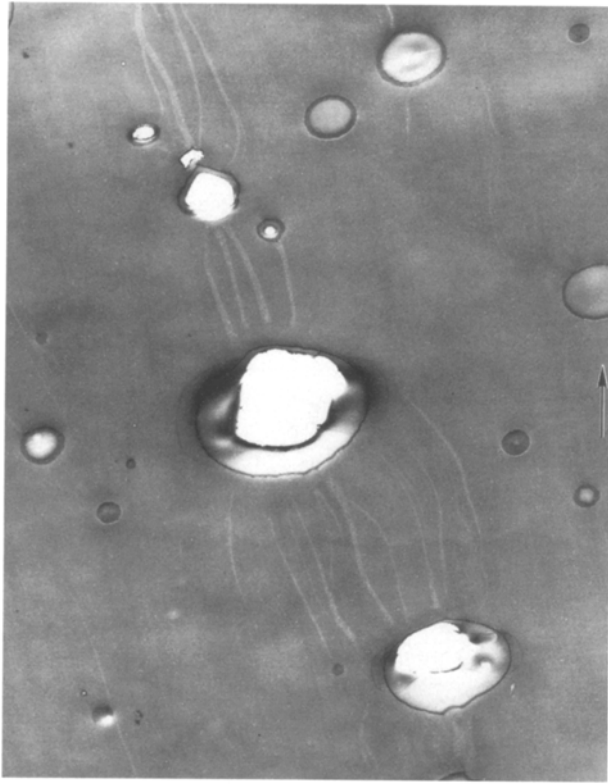
Figure 18 Transmission electron micrograph revealing craze-like damage in the fatigue-damage zone. This micrograph corresponds to the position T in Fig. 17a.
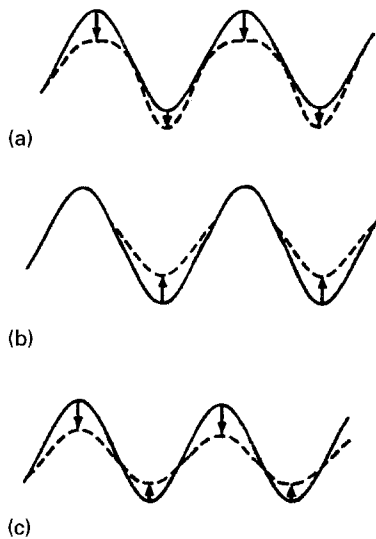

Figure 19 Effect of crack-tip shielding mechanisms on the fatigue driving force for rubber-modified epoxy polymers. (a) shielding via blunting, (b) shielding via closure, (c) total shielding.

respectively. A thin specimen from the mid-plane of the CT specimen was prepared and viewed using a light optical microscope. Fig. 20 shows the damage zone of the crack for several ΔK levels. This micrograph was obtained with reflective light and viewed under bright light. The larger zone, when viewed by naked eye, is a whitened zone indicative of cavitation. The smaller and brighter zone adjacent to the crack plane is the shear yielded zone. The latter is confirmed from higher magnification TOM micrographs,
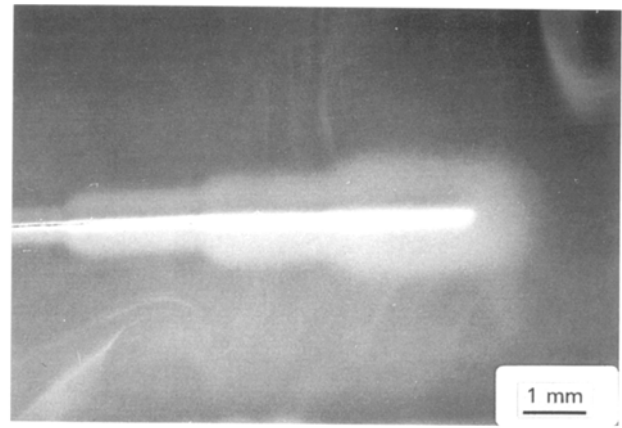

Figure 20 Optical micrograph showing the cavitation zone and the shear-yielded zone for DGEBA-550/Pip/CTBN(10) at four different ΔK levels.

as previously shown in Fig. 17a–c. The fact that the cavitation zone in CTBN-8-modified epoxies is larger than the size of the shear yielded zone is consistent with previous findings for static loading [10].

Measured values for the cavitation and plastic zones are given in Table III. Several equations have been proposed which predict a linear relation between the size of the plastic zone, $2r_y$, and $(K_{max}/\sigma_y)^2$. The slope of this linear relation is equal to 0.11, 0.32, and 0.39 for plane strain and plane stress equations of Irwin [24] and for Dugdale model [39], respectively. An evaluation for these models based on the slope of the plot of measured plastic-zone size, $2r_y$, versus $(K_{max}/\sigma_y)^2$ (see Fig. 21) confirms that this slope is smaller than 0.13 which is in good agreement with that from the Irwin plane-strain equation. Therefore, the use of the plane-strain plastic zone estimation of Irwin for describing the particle–plastic zone interactions in this material is justified. More importantly, because plane strain conditions hold, then A and m values reported in this paper are transferable (i.e. they can be used to rank materials and can be manipulated to predict long-term performance in the field through the stress intensity approach).

The relative size of the rubber cavitation zone to the matrix shear-yielded zone at different ΔK levels may be useful in detecting a plane strain to plane stress transition. Fig. 22 shows a plot of ratio of $2r_c/2r_y$ versus ΔK, where $2r_c$ is the size of the cavitation zone. As can be seen from this figure, the ratio of cavitation/shear yielding decreases with increasing ΔK. This result indicates that the relative amount of hydrostatic tension to deviatoric stress decreases with increasing ΔK which is consistent with the notion of plane strain to plane stress transition with increasing ΔK. It is noteworthy that the size of the cavitation zone measured for DGEBA-550/Pip/CTBN(10) is consistent with that measured by Pearson and Yee [10] for DGEBA-187/Pip/CTBN(10) who reported a cavitation zone size of 1500 µm for $K = 2$ MPa m$^{0.5}$.

Another valuable piece of information that can be obtained from the measurements for the cavitation zone is the average stress required for cavitated CTBN rubber-modified epoxy. Using the plane-stress

TABLE III Calculated plastic zone radius, r_y, from Equation 5, measured plastic zone radius, r_y^m, and measured cavitation zone radius, r_c, for the micrograph shown in Fig. 20. The tensile yield strength of the corresponding material is 56.5 MPa

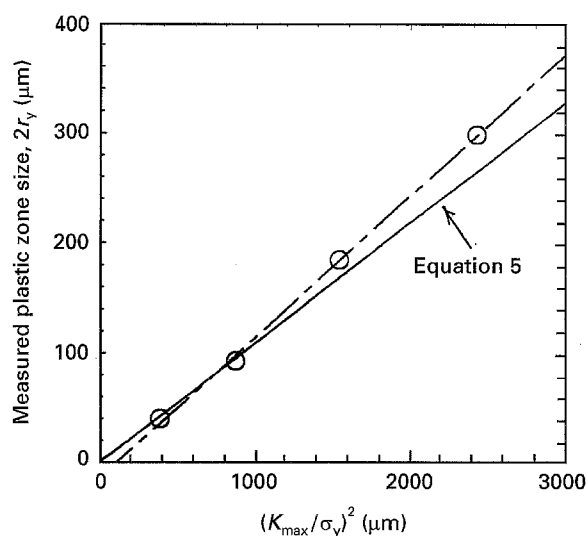| ΔK^a (MPa m$^{0.5}$)	r_y (μm)	r_y^m (μm)	r_c (μm)	r_y/r_c
1.0	20.5	20.0	325.0	0.062
1.5	46.0	46.5	567.5	0.082
2.0	82.0	93.0	800.0	0.116
2.5	128.0	150.0	1030.0	0.146

$^a R = 0.1$.

Figure 21 A plot of measured plastic zone versus $(K_{max}/\sigma_y)^2$. Note that the slope of this plot ($m = 0.13$) is in good agreement with $(2/6\pi)$ from plane strain equation (i.e. Equation 5).
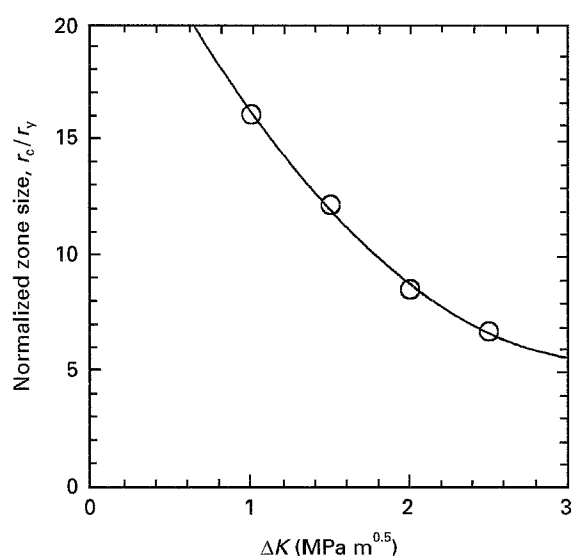

Figure 22 The ratio of cavitation zone size/plastic zone size versus ΔK.

equation of McClintock and Irwin [24], or the equation for the size of the cavitation zone by Zhang et al. [40], average values of 20 and 14 MPa were obtained, respectively. Both these values are in close agreement with the values reported by others [10,40].

4. Conclusions

Epoxy polymers modified by CTBN or MBS rubber particles were prepared with differing volume fractions of the modifiers. The FCP behaviour and the crack-tip shielding mechanisms operating under cyclic loading conditions were studied by careful examination of the fatigue-fracture surfaces and the sub-fatigue-fracture surfaces of fatigue samples, using SEM and TOM techniques. Furthermore, the sizes of the cavitation and plastic zones were measured for different ΔK levels. Based on the results obtained from this study, the following conclusions can be drawn.

1. Crack-tip plastic zone–rubber particle interactions induce a transition, ΔK_T, in the FCP behaviour in CTBN rubber-modified epoxy polymers. Consequently, rubber cavitation/shear banding and plastic void-growth mechanisms become active when the size of the plastic zone becomes large compared to the size of the rubber particles. As result, both neat and CTBN rubber-modified epoxies exhibit similar FCP resistance when $\Delta K < \Delta K_T$. Conversely, CTBN-modified epoxies show higher FCP resistance when $\Delta K > \Delta K_T$.

2. As a result of these interactions, the use of smaller 0.2 μm MBS particles in place of 1.5 μm CTBN particles results in about one order of magnitude improvement in FCP resistance of the rubber-modified system through the entire crack-growth regime.

3. The slope of the Paris–Erdogan power law depends on the volume fraction of the modifiers and not on the particle size or blend morphology.

4. While the rubber particle size and blend morphology strongly affect the near-threshold FCP behaviour, the volume fraction of the modifiers has no effect on threshold behaviour.

5. The measurements of the plastic zone sizes for CTBN-modified epoxy reveal that the formal plane-strain plastic-zone size of Irwin provides a reasonable estimate of both the size and the shape of the plane-strain plastic zone in CTBN-modified epoxy polymers.

References

1. F. J. McGARRY and A. M. WILLNER, Org. Coat. Plast. Chem. 28 (1968) 512.
2. N. J. SULTAN, R. C. LAIBLE and F. J. McGARRY, J. Appl. Polym. Sci. 6 (1971) 127.
3. W. D. BASCOM, R. L. COTTINGTON, R. L. JONES and P. PEYSER, J. Appl. Polym. Sci. 19 (1975) 2524.
4. S. KUNZ-DOUGLASS, P. W. R. BEAUMONT and M. F. ASHBY, J. Mater. Sci. 15 (1980) 1109.
5. A. J. KINLOCH, S. J. SHAW and D. L. HUNSTON, Polymer 24 (1983) 1355.
6. A. F. YEE and R. A. PEARSON, J. Mater. Sci. 21 (1986) 2462.

7. R. A. PEARSON and A. F. YEE, *ibid.* **21** (1986) 2475.
8. H. J. SUE and A. F. YEE, *ibid.* **24** (1989) 1447.
9. Y. HUANG and A. J. KINLOCH, *ibid.* **27** (1992) 2763.
10. R. A. PEARSON and A. F. YEE, *ibid.* **26** (1991) 3828.
11. A. G. EVANS, Z. B. AHMAD, D. G. GILBERT and P. W. R. BEAUMOUNT, *Acta Metall.* **34** (1986) 79.
12. C. K. RIEW, E. H. ROWE and A. R. SIEBERT, *ACS Adv. Chem. Ser.* **154** (1976) 326.
13. S. WU, *Polymer* **26** (1985) 643.
14. A. MARGOLINA and S. WU, *ibid.* **29** (1988) 2170.
15. A. S. HOLIK, R. S. KAMBOUR, S. HOBBS and D. FINK, *Microstruct. Sci.* **7** (1979) 357.
16. D. N. SHAH, J. A. MANSON, G. M. CONNELLY, G. ATTALLA and R. W. HERTZBERG, *ACS Adv. Chem. Ser.* **208** (1984) 117.
17. J. A. MANSON, R. W. HERTZBERG, G. M. CONNELLY and J. HWANG, *ibid.* **211** (1986) p. 291.
18. J. HWANG, J. A. MANSON, R. W. HERTZBERG, G. A. MILLER and L. H. SPERLING, *Polym. Eng. Sci.* **29** (1989) 1466.
19. *Idem, ibid.* **29** (1989) 1477.
20. J. KARGER-KOCSIS and K. FRIEDRICH, *Colloid Polym. Sci.* **270** (1992) 549.
21. D. TAYLOR, "Fatigue Thresholds" (Butterworth, 1984).
22. S. USAMI, in "Fatigue Threshold" (EMAS, Warley, UK) p. 205.
23. H. R. AZIMI, R. A. PEARSON, and R. W. HERTZBERG, *J. Mater. Sci. Lett.* **13** (1994) 1460.
24. F. A. McCLINTOCK and G. R. IRWIN, ASTM STP 381, (American Society for Testing and Materials, Philadelphia, PA, 1965) p. 84.
25. G. R. YODER, L. A. COOLEY and T. W. CROOKER, "Titanium 80", edited by H. Kimura and O. Izumi, Vol. 3 (AIME, Warrendale, PA, 1980) p. 1865.
26. M. GUPTA, K. BOWO, E. J. LAVERINA and J. C. EARTH-MAN, *Scripta Metall.* **28** (1993) 1053.
27. S. KUMAI, K. YOSHIDA, Y. HIGO and S. NUNOMURA, *Int. J. Fatigue* **14** (1992) 105.
28. K. P. GADKAREE and G. SALEE, *Polym. Compos.* **4** (1983) 19.
29. R. W. HERTZBERG, in "Deformation and Fracture Mechanics of Engineering Materials", 3rd Edn (Wiley, New York, 1989) p. 517.
30. R. BAGHERI, PhD dissertation, Lehigh University, (1995).
31. J. Y. QIAN, R. A. PEARSON, V. L. DIMONIE and M. S. EL-AASSER, *PMSE ACS* **70** (1994) 17.
32. R. O. RITCHIE, *Mater. Sci. Eng.* **A103** (1988) 15.
33. Z. B. AHMAD, M. F. ASHBY and P. W. R. BEAUMONT, *Scripta Metall.* **20** (1986) 843.
34. A. LAZZERI and C. B. BUCKNALL, *J. Mater. Sci.* **28** (1993) 6799.
35. M. D. GLAD and E. J. KRAMER, *ibid.* **26** (1991) 2273.
36. H. J. SUE, *ibid.* **27** (1992) 3098.
37. R. A. PEARSON and A. F. YEE, *ibid.* **24**, (1989) 2571.
38. A. G. EVANS and R. M. CANNON, *Acta Metall.* **34** (1986) 761.
39. D. S. DUGDALE, *J. Mech. Phys. Solids* **8** (1960) 100.
40. X. C. ZHANG, C. B. BUCKNALL, M. L. ORTON and G. V. JACKSON, in "9th International Conference on Deformation Yield and Fracture in Polymers", Churchill College, Cambridge, UK, April 1994, p. 63/1.